Slightly rarefied gas flows over a sphere

Chunpei Cai and Quanhua Sun

Citation: AIP Conference Proceedings **1628**, 770 (2014); doi: 10.1063/1.4902671
View online: http://dx.doi.org/10.1063/1.4902671
View Table of Contents: http://scitation.aip.org/content/aip/proceeding/aipcp/1628?ver=pdfcov
Published by the AIP Publishing

Slightly Rarefied Gas Flows Over a Sphere

Chunpei Cai* and Quanhua Sun†

*Department of Mechanical and Aerospace Engineering, New Mexico State University
Las Cruces, New Mexico, 88001 USA,
†State Key Laboratory of High Temperature Gas Dynamics, No.15 Beishihuanxi Road
Institute of Mechanics, Chinese Academy of Sciences, Beijing, 100190 China

Abstract. The problem of near continuum gas flows over a sphere is investigated numerically. Three types of surface boundary conditions are adopted: 1) non-slip and constant temperature surface; 2) velocity slip with velocity gradient but without temperature gradient along the surface; and 3) velocity slip with considerations of both velocity gradient (along the direction normal to the surface), as well as temperature gradient along the surface. Navier-Stokes equations for compressible flows are solved with the Roe scheme. The numerical results include coefficient distributions for surface pressure, friction, heat flux, velocity slip, and temperature jump. The third type surface boundary condition does not create significant differences from the second type.

Keywords: Flow Dynamics, flow computation, Navier-Stokes equations, slip flows
PACS: 47.45.-n, 47.11.-j, 47.10.ad, 47.45.Gx

INTRODUCTION

Gas flow over a sphere is a fundamental fluid dynamic problem with numerous applications. Examples include, but are not limited to, i) droplets or particulate matters in smog; ii) liquid droplets during a spray; iii) aluminium powders in combustion chambers; iv) solar winds passing a moon without gravity; v) mixing processes in chemical engineering; and vi) heavy materials separation in nuclear engineering.

Many of them are related to rarefication effects, which can be expressed with the Knudsen (Kn) number[1]:

$$Kn = \lambda/L, \lambda = 1/(\sqrt{2}\pi d^2 n), \tag{1}$$

where λ is the mean free path based on the hard sphere model, L a characteristic length, d the molecular diameter, and n the number density. According to different Kn numbers, flows can be classified as: i) continuum flow ($Kn < 0.001$) which can be solved by the Navier-Stokes Equations (NSEs) and the conditions of non-slip, constant temperature/heat flux at the surface; ii) slip flow ($0.001 < Kn < 0.01$), where the NSEs are still applicable but the boundary conditions at the surface shall be modified by considering some gradient effects, examples include flows related with Micro-Electro-Mechanical Systems (MEMS); iii) transitional flows ($0.01 < Kn < 10$), for most gas flows, numerical simulations shall be used for investigations; and iv) free molecular flows ($Kn > 10$), where both numerical and analytical results are applicable. The current status for development of low speed sphere flows can be summarized as follows: i) in the continuum flow regime, there are many successful investigations, numerically, theoretically, and experimentally; ii) in the slip flow regime, there are some recent developments for numerical and experimental investigations which provide some new insights; iii) in the transitional flow regime, almost all studies are numerical simulations; for example, with the direct simulation Monte Carlo (DSMC) [1] method; and iv) free molecular flow, surface properties[2] for a diffuse or a specular reflective sphere were obtained about half a century ago analytically. The flowfield properties (i.e., density, velocity, pressure and temperature), were investigated with the gaskinetic methods, and some such analytical methods are documented [3]. However, only recently[4] the detailed flowfield properties for flows over a diffuse reflective sphere were evaluated and validated with DSMC simulations.

In this paper, the problem of slightly rarefied gas flows over a sphere will be investigated numerically. In the literature, theoretical studies are rare, and there are scarce numerical studies with different simplifications.

The next sections are organized as follows: in section II, a detailed problem statement, governing equations, boundary conditions and numerical schemes will be provided; in section III, many comparisons and discussions will be performed, and in the last section, summaries and conclusions from the work will be drawn.

Proceedings of the 29th International Symposium on Rarefied Gas Dynamics
AIP Conf. Proc. 1628, 770-777 (2014); doi: 10.1063/1.4902671

PROBLEM DESCRIPTIONS AND NUMERICAL SIMULATION SCHEME

The problem is illustrated as Fig.1: slightly rarefied, or near continuum, gas flows over a sphere. The flowfield is symmetric; hence, only the upper flowfield is studied. There are three boundaries: i) free stream flows entering the outer circular boundary with a radius of R_2, with given flowfield properties, e.g., ρ_∞, U_∞, T_∞, and p_∞; ii) symmetric center lines; and iii) sphere surface with boundary conditions of nonslip/slip velocity and constant/jump temperature.

To be general, compressibility with different free stream Mach numbers will be considered, including the density equation. A full set of NSEs are adopted to solve the coupling flow and temperature fields simultaneously with density, flowfield velocity, and temperature, ρ, U, V, and T. The flow is essentially axisymetric, and its governing equations are:

$$\frac{\partial U}{\partial t}+\frac{\partial (E_{in}-E_v)}{\partial x}+\frac{\partial (F_{in}-F_v)}{\partial r}=\frac{G}{r}, \tag{2}$$

$$U=\begin{pmatrix}\rho\\ \rho u\\ \rho v\\ E\end{pmatrix}, E_{in}=\begin{pmatrix}\rho u\\ \rho u^2+p\\ \rho uv\\ u(E+p)\end{pmatrix}, F_{in}=\begin{pmatrix}\rho v\\ \rho uv\\ \rho v^2+p\\ v(E+p)\end{pmatrix}, \tag{3}$$

$$E_v=\begin{pmatrix}0\\ \tau_{xx}\\ \tau_{xr}\\ u\tau_{xx}+v\tau_{xr}+q_x\end{pmatrix}, F_v=\begin{pmatrix}0\\ \tau_{xr}\\ \tau_{rr}\\ u\tau_{xr}+v\tau_{rr}+q_r\end{pmatrix}, G=\begin{pmatrix}-\rho v\\ \tau_{xr}-\rho uv\\ \tau_{rr}-\tau_{rx}-\rho v^2\\ u\tau_{xr}+v\tau_{rr}+q_r-v(E+p)\end{pmatrix}, \tag{4}$$

where

$$\begin{array}{lll}\tau_{xx}=-\frac{2}{3}\mu\left(2\frac{\partial u}{\partial x}-\frac{\partial v}{\partial r}-\frac{v}{r}\right), & \tau_{rr}=-\frac{2}{3}\mu\left(2\frac{\partial v}{\partial r}-\frac{\partial u}{\partial x}-\frac{v}{r}\right), & \tau_{xr}=\mu(\frac{\partial u}{\partial r}+\frac{\partial v}{\partial x})\\ \tau_{rx}=-\frac{2}{3}\mu\left(\frac{\partial u}{\partial x}+\frac{\partial v}{\partial r}+\frac{v}{r}\right), & q_x=k\frac{\partial T}{\partial x}, & q_r=k\frac{\partial T}{\partial r},\end{array} \tag{5}$$

where E is internal energy. The above formulas are similar to the two-dimensional governing equations; the differences include several extra terms within the shear stress tensor and extra source terms.

The variable hard sphere (VHS) model [1] is used to model the viscosity variations with temperature, and the thermal conductivity coefficient k changes correspondingly:

$$\mu(T)=\mu_{ref}\left(T/T_{ref}\right)^{\omega_1}, k(T)=\frac{\gamma R}{\gamma-1}\frac{\mu}{Pr}. \tag{6}$$

The equation of state is adopted to link the pressure, temperature and density.

The boundary conditions for the problem are listed as:

$$\begin{array}{llll}T=T_\infty; & p=p_\infty; & U=U_\infty, \rho=\rho_\infty; & \text{farfield,}\\ v=0; & \frac{\partial u}{\partial r}=\frac{\partial P}{\partial r}=0; & \frac{\partial T}{\partial r}=0, & \text{symmetric line at the bottom.}\end{array} \tag{7}$$

For the sphere surface boundary conditions, there are some differences. For convenience, the sphere surface is described by using the planar polar coordinate variables (n,θ), at the surface only:

$$u_n=0, \quad u_\theta=0, \quad T_g=T_w, \quad \text{non-slip and constant temperature,} \tag{8}$$

$$u_n=0; \quad u_\theta=K_1\frac{\partial u_\theta}{\partial n}+\frac{K_2}{T_g}\frac{\partial T_g}{\partial s}, \quad T_g-T_w=K_3\frac{\partial T_g}{\partial n}, \text{velocity slip \& temperature jump at sphere surface,} \tag{9}$$

where R_1 is the sphere radius, and

$$K_1=\frac{2-\sigma_M}{\sigma_M}\lambda; K_2=\frac{3}{4}\nu; K_3=\frac{2-\sigma_T}{\sigma_T}\frac{2\gamma}{\gamma+1}\frac{\lambda}{Pr}. \tag{10}$$

Because there is almost no temperature variation in the flowfield, for simplicity, Eqn. 1 is used to compute the mean free path. It is also worthy of mentioning that the velocity slip boundary modeling may have different implementations[5], and there may be slight differences in the simulation results.

In the past, in the velocity slip and temperature jump boundary formulas, Eq.9, the term with $\partial T/(R_1\partial\theta)$ was considered to be smaller than the velocity gradient term $\partial u/\partial n$; hence, it is usually set to zero for simplicity. In this

work, such a treatment is denoted as a "partial slip" surface model. A more comprehensive model with both velocity and temperature gradients is also investigated as a "fully slip" surface model. The latter preserves the temperature gradient $\partial T/\partial s$ because around the front stagnation point, the velocity is zero, while the temperature is the highest; hence, some temperature variations along the front side of sphere surface are expected, and may contribute to the slip velocity. One major goal of this paper is to compare the consequences due to the latter two different boundary conditions.

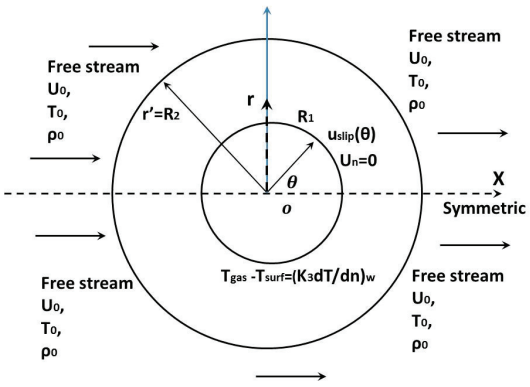

FIGURE 1. Model schematic: sphere (cut through) and boundary conditions.

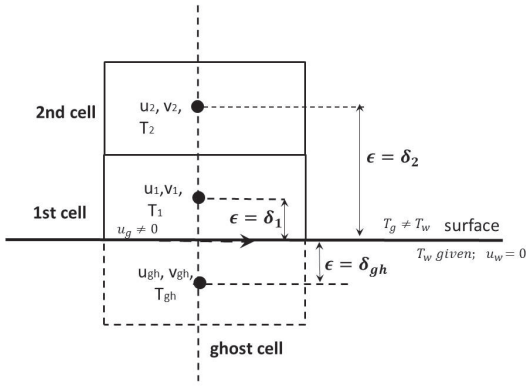

FIGURE 2. Illustration for near surface ghost cell treatment.

The numerical simulation scheme in this work was the Roe's approximate Riemann solver [6, 7]. The flow field is divided into small cells, and the finite volume method is adopted for the simulation. Ghost cells are distributed along the four boundaries, and the one at the wall surface is illustrated as Fig.2. At the surface, the gas velocity u_g and temperature T_g are not the same as the corresponding surface properties, and will be updated at each step.

The flowfield properties are updated with the following two steps of time marching scheme:

$$U_{ij}^{n+1/2} = U_{ij}^{n} + \frac{\Delta t}{2}\mathrm{Res}_{ij}{}^{n}, U_{ij}^{n+1} = U_{ij}^{n+1/2} + \frac{\Delta t}{2}\mathrm{Res}_{ij}{}^{n+1/2}, \tag{11}$$

where Res_{ij}^{n} is the residual for cell ij at time step $t = n\Delta t$.

The treatment of the wall boundary conditions in this work is crucial. For the non-slip boundary condition, the velocity and temperature gradients are important properties, and are handled with second order extrapolations. **At locations sufficiently close to the surface**, the velocity is nonslip and can be assumed to behave as:

$$u(\varepsilon) = a + b\varepsilon + c\varepsilon^2; u(\varepsilon = 0) = 0, u(\varepsilon = \delta_1) = u_1, u(\varepsilon = \delta_2) = u_2, \tag{12}$$

where ε is the distance from the sphere surface along the normal direction; and δ_1, δ_2 are the distances from the surface to the center of the 1st and 2nd layers of cells (see Fig.2) with two computed properties $u_1(\varepsilon = \delta_1)$, $u_2(\varepsilon = \delta_2)$ at the

centers for two cells adjacent to the wall. The coefficients of a, b, and c can be derived, and $b = \partial u/\partial \varepsilon$ at the surface is the desired velocity gradient. The ghost cell properties are updated to satisfy the nonslip and constant temperature boundary conditions:

$$u_{gh}(\varepsilon = -\delta_1) = -u(\varepsilon = \delta_1), v_{gh}(\varepsilon = -\delta_1) = -v(\varepsilon = \delta_1), T_{gh}(\varepsilon = -\delta_1) = 2T_w - T(\varepsilon = \delta_1). \tag{13}$$

For the velocity slip and temperature jump boundary conditions, the temperature solution shall be solved first as its gradient presents in the velocity slip boundary conditions. It can be assumed that **at locations sufficiently close to the sphere surface**, the relation between the temperature and its gradient is also generally applicable; hence, the 3rd formula in Eqn.9 can be treated as a first order ordinary differential equation (along the normal n-direction) for the temperature, and the solution for temperature is:

$$T_g(\varepsilon) = (T_g(\delta_1) - T_w)\, e^{(\varepsilon - \delta_1)/K_3} + T_w, \tag{14}$$

where $T_g(\delta_1)$ is the corresponding gas bulk temperature at the center for the first layer cells. Then it is evident that:

$$\frac{dT_g}{dn}|_{\varepsilon=0} = \frac{e^{-\delta_1/K_3}}{K_3}\,(T_g(\delta_1) - T_w)\,, \tag{15}$$

or may be obtained from Eqn. (9) quite conveniently. After this step, all the gas temperature gradients along the surface $\partial T/(R_1 \partial \theta)$ at each station are computed with the solved neighboring temperature values along the surface.

For the "partial" velocity slip model, the treatment for the velocity is quite similar with the temperature distributions. The 2nd formula in Eqn. 9 can be considered as a 1st order ordinary differential equation as well, and the solution is:

$$u_\theta(\varepsilon) = u_\theta(\delta_1) e^{(\varepsilon - \delta_1)/K_1}, \tag{16}$$

correspondingly, for the "full" slip model which includes the temperature gradient term, the solution is:

$$u_\theta(\varepsilon) = u_\theta(\delta_1) e^{(\varepsilon - \delta_1)/K_1} + \left(\frac{K_2}{T_g}\frac{\partial T_g}{\partial s}\right)|_{\varepsilon=0}. \tag{17}$$

The above semi-analytical formulas only require some inputs from the 1st and the 2nd cells adjacent to the surface; hence, the computations are quite simple. Temperature, velocity, and their gradients at the surface are interrelated and the boundary effects to the flowfield are via the flux contributions from the ghost cells.

RESULTS AND DISCUSSIONS

Several simulations were performed, with those three types of surface boundary conditions. During the simulations, R_2 is set to $20R_1$, the Mach number is set to small values to achieve an incompressible flow state, and the Kn number is set to between 0.001 and 0.01 within the velocity slip and temperature jump regime. The simulation results obtained with nonslip boundary conditions are for comparison, while the simulation results using the slip boundary condition are more reliable. A 200×200 mesh size along the circumferential and radial directions is adopted to discrete the flowfield, and mesh convergency examinations indicate such a mesh size is sufficient to resolve the flowfield. Figure 3 shows the residual development histories during one set of numerical simulations with the three kinds of velocity boundary conditions, with $Kn = 0.001$ and $Ma = 0.05$. There are minor differences among the three curves; however, they are not appreciable when plotted in log-scales. The residuals decrease almost eight orders and convergence is evident. It shall be reminded that both axis are plotted in log scales. The X-axis is normalized by the characteristic time, while the y-axis by the free stream pressure:

$$t^* = t/(R_1/U_\infty), p^* = \frac{1}{p_\infty}\sqrt{\frac{1}{N_{cell}}\sum_{i=1}^{N_{cell}}(\Delta p)_i^2}. \tag{18}$$

Figure 4 shows the normalized pressure distributions with the full velocity slip boundary condition model with a combination of parameter, $Kn = 0.001$ and $Ma = 0.05$. The stagnation pressure is slightly larger than other locations, and the smallest pressure adjacent to upper right surface indicates larger flow velocity and possible flow separation.

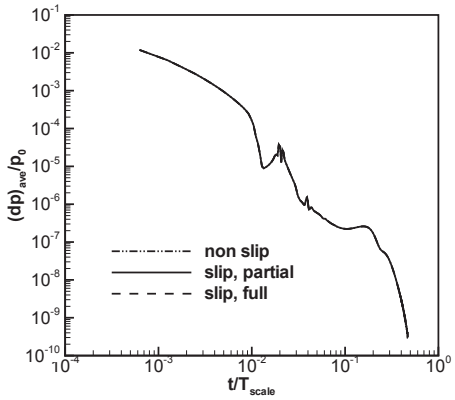

FIGURE 3. Numerical simulation residual development histories: $Kn = 0.001$ and $Ma = 0.05$.

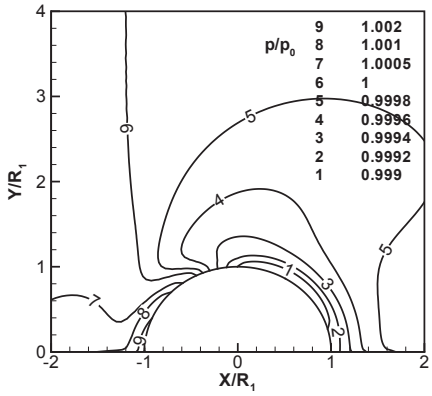

FIGURE 4. Normalized pressure distributions, p/p_0, full velocity slip condition, $Kn = 0.001$ and $Ma = 0.05$.

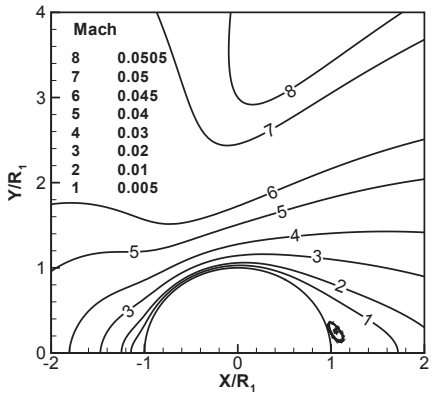

FIGURE 5. Mach number contours, full velocity slip condition, $Kn = 0.001$ and $Ma = 0.05$.

Figure 5 shows the Mach number contours with the model of full velocity slip boundary condition. In front of the sphere, flows are compressed or squeezed, due to the narrower passage; hence, the streamline gradient along the sphere normal direction varies. The streamlines are not only functions of θ, but also of r and other variables. At the backside of the sphere, especially the "dead water" zone with vortex circulations, the average Mach number decreases. Evidently, as shown in this figure, flow separations occur on the surface and a small vertex is presented. Figure 6 shows the normalized v- velocity component, with the full slip boundary condition. These contours change from positive to negative values; hence, this figure is one of the most effective ones to show the flowfield variations.

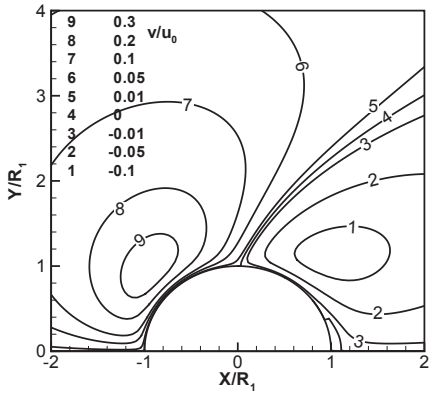

FIGURE 6. Normalized velocity component v/U_0, full velocity slip condition, $Kn = 0.001$ and $Ma = 0.05$.

The above three figures are for the combinations of $Kn = 0.001$ and $Ma = 0.05$ with full velocity slip boundary conditions, while the next five figures present various surface properties by comparing the partial and full slip boundary conditions. Figure 7 shows sphere surface pressure distributions, $C_p(\theta) = (p(\theta) - p_\infty)/(\rho_\infty U_\infty^2/2)$, for the non slip, partial and full slip boundary conditions. Essentially there are no appreciable differences. Figure 8 shows the normalized surface friction distributions, $C_f(\theta) = \tau(\theta)/(\rho_\infty U_\infty^2/2)$, the peak values are quite smaller than the peak values for surface pressure distributions. The friction coefficient for the non slip boundary condition is significantly larger than the slip boundary condition results. A larger shear stress coefficient at the front side indicates larger velocity changes in the local flowfield; and $C_f = 0$ around 140° reflects a flow separation there. Figure 9 shows the sphere surface heat transfer coefficient $C_q(\theta) = k(\partial T/\partial n)/(\rho_\infty U_\infty^3/2)$. The heat flux for the non-slip boundary case has much larger value than the slip boundary condition results; this may be due to the larger friction. Equation 9 indicates that for both the partial and full flip scenarios, the heat flux is proportional to the surface temperature gradient which are proportional to the temperature differences at the surface. The stagnation temperature is the highest, representing the highest heat flux from the stagnation point to the flowfield. Figure 10 shows normalized sphere surface slip velocities, $u_g(0)/u_\infty$;and the differences between the partial-slip and full-slip conditions are small. Along the surface, at around of $\theta \approx 140^\circ$, the slip velocity value changes signs, reflecting a flow separation. Figure 11 shows the normalized temperature jump along the sphere surface, $(T_g(\varepsilon = 0) - T_w)/T_w$; and Eq. 9 shows that the temperature is actually proportional to the local gradients, and the full and partial slip velocity boundary conditions yield similar patterns. The temperature and its gradient are closely linked; one property can lead to the other.

The following Fig. 7–Fig.11 illustrate that the full and partial velocity slip conditions create almost identical flow field and surface property patterns, only small differences in the slip velocity. This indicates that the term containing the temperature gradient $\partial T/\partial s$, in Eq. 9, provides minor contributions to the flow solutions. However, as shown, slip and non-slip boundary conditions truly create different results of larger friction and heat flux at the wall.

SUMMARY

This paper included investigations on compressible, near continuum gas flows over a sphere. Three types of boundary conditions, nonslip, partial and full slips, were incorporated with the full set of Navier-Stokes equations. The simulation parameters are within special Kn and Ma numbers, to achieve the near continuum and incompressible flows. The numerical scheme was the Roe's approximate solver for the non-viscous convection flux, while the viscous flux

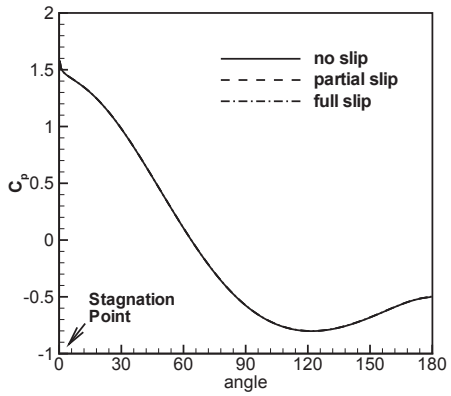

FIGURE 7. Sphere surface pressure coefficients, C_p, $Kn = 0.001$ and $Ma = 0.05$.

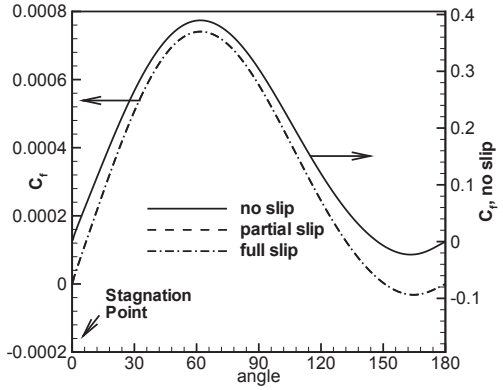

FIGURE 8. Sphere surface friction coefficients, C_f, $Kn = 0.001$ and $Ma = 0.05$.

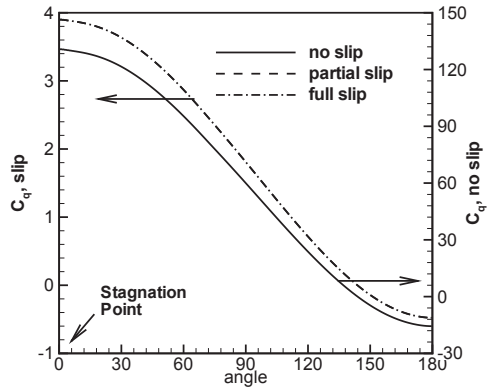

FIGURE 9. Sphere surface heat transfer coefficients, C_q, $Kn = 0.001$ and $Ma = 0.05$.

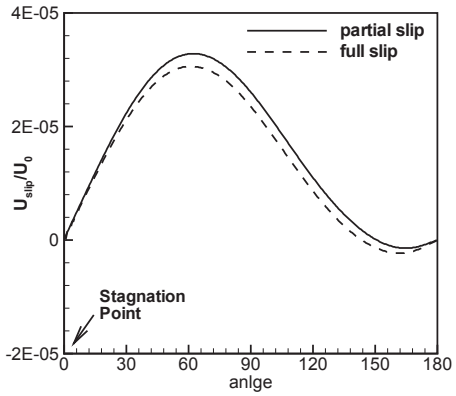

FIGURE 10. Normalized sphere surface slip velocity, $Kn = 0.001$ and $Ma = 0.05$.

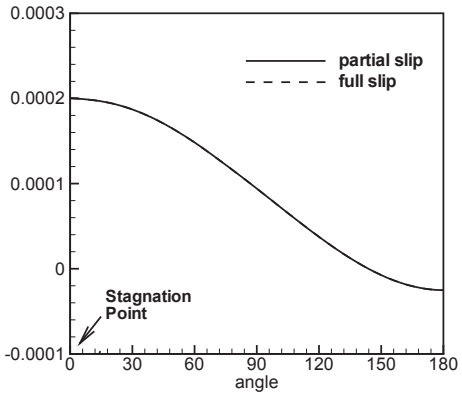

FIGURE 11. Normalized temperature jump at the sphere surface, $Kn = 0.001$ and $Ma = 0.05$.

contributions are treated as source terms. The treatment of boundary conditions created several analytical solutions for the temperature and velocity at locations close to the sphere surface.

This study investigated the flow and temperature fields without the many assumptions and simplifications adopted by many other papers in the literature. The results indicated that different slip boundary conditions have minor effects on the flowfield and surface properties. However, adoptions of velocity slip and non-slip boundary conditions create quite differences in the surface friction and heat flux coefficients.

REFERENCES

1. G. Bird, *Molecular Gasdynamics and Numerical Simulation Methods*, Oxford University Press, Oxford, UK, 1994.
2. S. Schaaf, and P. Chamber, *Flow of Rarefied Gases*, Princeton University Press, New Jersey, 1961.
3. C. Cercignani, *Rarefied Gas Dynamics: From Basic Concepts to Actual Calculations*, Cambridge University Press, New York, 2000.
4. C. Cai, and K. Khasawneh, *Journal of Spacecraft and Rockets* **46**, 1124–1131 (2009).
5. R. Myong, *Physics of FLuids* **16**, 104 (2004).
6. P. Roe, *Journal of Computational Physics* **43**, 357–372 (1981).
7. C. Hirsch, *Numerical Computation of Internal and External Flows*, Wiley and Sons, Hoboken, New Jersey, 2002.